Eu-MOF-Based Fluorescent Ratiometric Sensor by Detecting 3,4,5-Trihydroxybenzoic for Fingerprint Visualization on Porous Objects

Muwen LIANG[1,2], Yabin ZHAO[1], Yaping LUO[1*], Bin DU[2], Wei HU[2], Bing LIU[2], Xihui MU[2], and Zhaoyang TONG[2*]

[1]*Department of Investigation, People's Public Security University of China, Beijing 100038, China*

[2]*State Key Laboratory of NBC Protection for Civilian, Beijing 102205, China*

[*]Corresponding authors: Yaping LUO and Zhaoyang TONG E-mail: yaping_luo@126.com and billzytong@126.com

Abstract: Latent fingerprints (LFPs) at the crime scene are served as important clues to locate the trajectory of criminal behavior and portray the characteristics of the suspect. Therefore, visualizing LFPs is of considerable significance. In this work, the europium metal-organic framework (Eu-MOF) sensor was successfully constructed for sensitive detection of gallic acid (3,4,5-trihydroxybenzoic acid, GA) and visualization of the sweat LFPs. The boric-acid-modified Eu-MOF was prepared by using the simple one-pot solvothermal method using Eu as the metal ion center and 3,5-dicarboxybenzeneboronic acid (BBDC) as the organic ligand. The sensor showed desirable photoluminescent performance through the chelating of BBDC with Eu^{3+}. The sensor exhibited the satisfactory linear relationship to GA in the range of 1 nM to 20 nM with a low detection limit of 0.34 nM under the optimized conditions. The prepared sensor with ideal selectivity to GA was successfully applied for visualizing LFPs on porous substrates with the high contrast and superior stability. Given the good performance of the sensor, all fingerprint images obtained from 1 200 samples presented clear friction ridges and met the identification criteria. Notably, the sensor had less impact on the subsequent deoxyribonucleic acid (DNA) detection, displaying a promising perspective for applications in extracting physical evidence of site investigation.

Keywords: Europium metal-organic framework (Eu-MOF); photoluminescence; 3,4,5-trihydroxybenzoic; latent fingerprints (LFPs) development.

Citation: Muwen LIANG, Yabin ZHAO, Yaping LUO, Bin DU, Wei HU, Bing LIU, *et al*., "Eu-MOF-Based Fluorescent Ratiometric Sensor by Detecting 3,4,5-Trihydroxybenzoic for Fingerprint Visualization on Porous Objects," *Photonic Sensors*, 2024, 14(1): 240127.

1. Introduction

In forensic science, the transfer of trace evidence during the course of criminal activities can provide vital investigative information that links people, locations, and objects. Latent fingerprints (LFPs) are the important type of trace evidence, since they are easily transferred and can identify an individual using the ridge patterns. Therefore, visualizing LFPs in the effective manner is of considerable significance [1]. More attentions were paid to the field of visualizing LFPs by the sensor responding substance composition involved in friction ridges, and the consequences that may have effect on the

Received: 28 April 2023 / Revised: 25 September 2023

DOI: 10.1007/s13320-024-0699-z
Article type: Regular

interpretation of the evidence at the judicial trial level [2–5].

Gallic acid (3,4,5-trihydroxybenzoic acid, GA) is a phenolic compound with two functional groups (hydroxyl groups and carboxylic acid group), exhibiting chemical activities of hydroxybenzoic acid and polyphenols. Meanwhile, GA is a secondary metabolite presenting in body fluids, including sweat [6]. The development methods of LFPs were mainly attributed to the sensing metabolite substances contained in sweat, such as amino acid and metal ions. GA is easily neglectable as a target component in the process of fingerprint development. Up to now, there are few relevant works reported visualizing LFPs by GA. The boronic moiety can interact with the hydroxybenzoic structure of GA through the covalent bonding between the phenolic hydroxyl group of the benzene ring with the hydroxyl group of the boric acid [7, 8]. Therefore, boronic acid can serve as promising functional monomers for establishing a general approach for detecting GA.

Metal-organic frameworks (MOFs) with rare earth ions as the metal center are porous crystalline materials that have been studied and applied in the fields of energy storage, catalysis, and separation. Rare earth MOFs have the advantages of MOF materials in addition to the rare earth metal ion 4f electronic layer, large orbital coupling effect, and internal magnetic anisotropy. Rare earth MOFs have higher coordination numbers and richer coordination geometries than transition metal ions as functional metal centers of MOFs due to the 4f electron layer of trivalent lanthanide ions [9]. Rare earth doped MOFs with special optical and electrical properties exhibited great prospects for the application of revealing fingerprints [10–19]. For instance, Jiang *et al*. [20] designed a ratio metric fluorescence (FL) biosensor based on the nanohybrids and enzyme-catalyzed reaction, with a structure of the black phosphorus quantum dots (BPQDs)-doped MOF realizing efficient detection of baicalin (BAI) in the solution, flexible substrate, and LFPs. Besides, Sun *et al*. [21] developed a lanthanide doped MOF (Ln-MOF) to respond to common nitro explosives through the phenomenon of FL quenching and realized its application in developing sweat-sebum LFPs on different impermeable surfaces successfully via the powder dusting method. Although some literature about lanthanide-containing fluorescent MOFs has been reported, there remain challenges to develop sensing strategies based on Ln-MOFs for visualizing LFPs with high contrast and stability responsiveness.

Based on the above, the boric-acid-modified Eu-MOF is synthesized by the solvothermal method to detect GA in LFPs, and the diagram of the mechanism for GA detection is illustrated in Fig. 1. Revealing LFPs in the crime scene is critical for suspect identification in the field of forensic science.

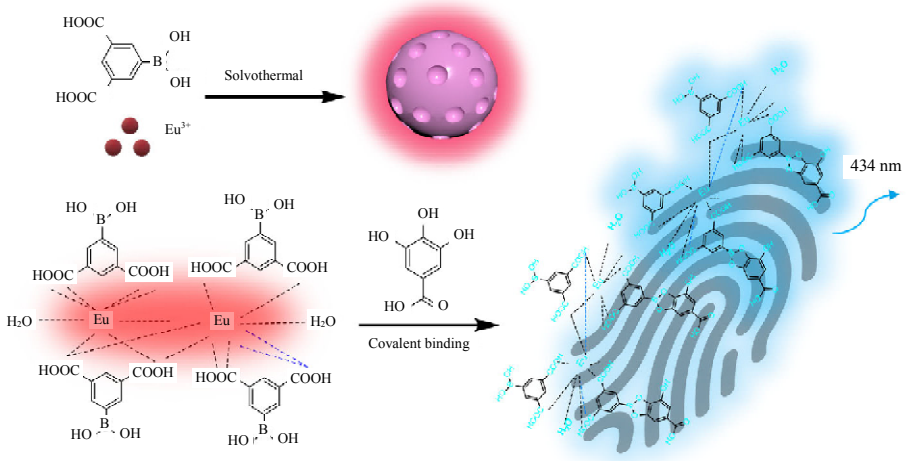

Fig. 1 Scheme of the preparation of Eu-MOF and the detection mechanism of GA.

In this work, our strategy is focused on fingerprints visualization by an effective approach. The strategy, achieving the visualization of fiction ridges of fingerprints, provides a starting perspective for public security authorities to carry out personnel traceability based on informatization investigation in the digital era.

2. Experiment

2.1 Preparation of Eu-MOF

The boric acid-functional Eu-MOF was prepared via a simple optimized solvothermal method. $EuCl_3 \cdot 6H_2O$ (0.4 mM) and 3,5-dicarboxybenzeneboronic acid (BBDC) (0.2 mM) were mixed and vigorously stirred for 18 min in the N,N-dimethylformamide (DMF, AR)/H_2O solution (V:V=7:3). The above reaction solution was transferred to the Teflon stainless-steel polytetrafluoroethylene (PTFE) autoclave and heated at 130 ℃ for 14 h. The product was cooled at room temperature, and then washed three times by centrifugation with DMF and ethanol, respectively. The white powder of the Eu-MOF was obtained after drying in the vacuum oven at 60 ℃ overnight.

2.2 Characterization of Eu-MOF

The as-synthesized MOF, Eu-BBDC@MOF, was characterized via the powder X-ray diffraction (PXRD), X-ray photoelectron spectroscopy (XPS), and scanning electron microscope (SEM). From Fig. 2(a), the SEM image shows that the obtained Eu-MOF exhibited the uniform dispersion with an average diameter of 1 μm. Moreover, the spherical structure of the Eu-BBDC@MOF with irregular holes on the surface can be considered to increase the contact area of the sensor with the surface. Due to its larger superficial area for high efficiency, the hollow ones were chosen for the further work. Besides, the PXRD pattern of Eu-BBDC@MOF was recorded and accorded well with the patterns of the

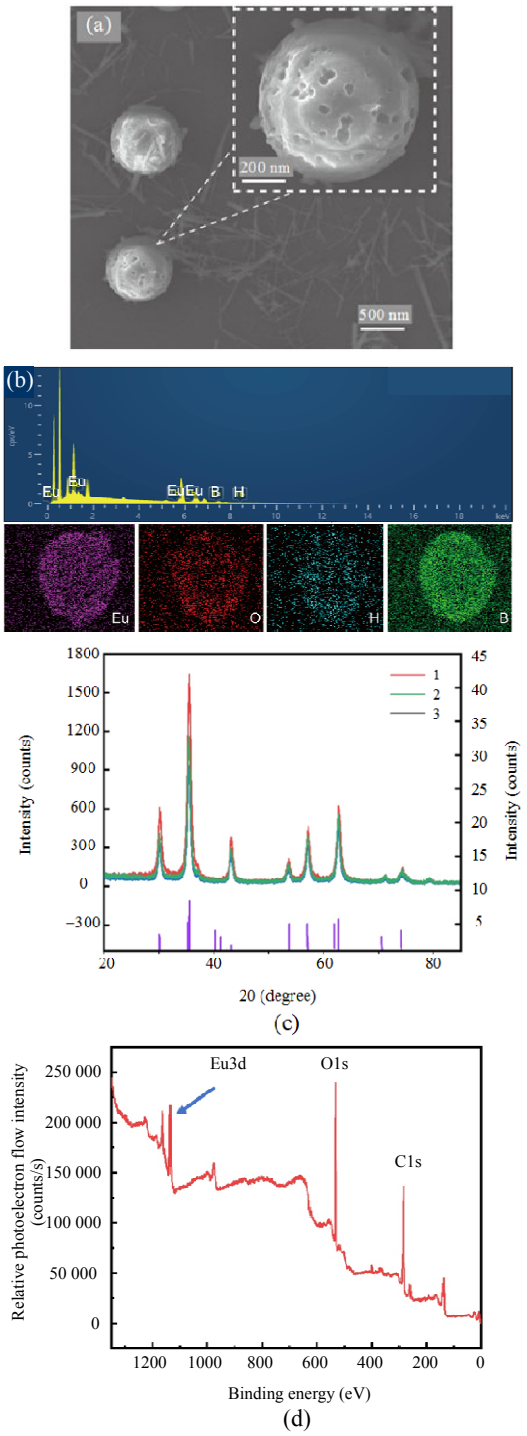

Fig. 2 Evaluation of the Eu-MOF: (a) morphological characterization of the Eu-MOF; (b) PXRD spectra of the Eu-MOF and Eu-MOF detecting GA (10 nM); (c) energy dispersive spectroscopy (EDS) mapping of Eu-MOF: elemental distribution of Eu, B, O, and H of the Eu-MOF under different scan rates: 40 $mV \cdot s^{-1}$, 60 $mV \cdot s^{-1}$, 80 $mV \cdot s^{-1}$, 100 $mV \cdot s^{-1}$, 120 $mV \cdot s^{-1}$, 140 $mV \cdot s^{-1}$, 160 $mV \cdot s^{-1}$, and 180 $mV \cdot s^{-1}$, respectively; 1 and 2 for the Eu-MOF and Eu-MOF mixed GA, and 3 for the crystalline reference; (d) XPS of Eu-MOF.

Eu-MOF [22] [Fig. 2(b)], which showed that the material can be retained well after it was immersed in H_2O for seven days or stored in the solid state at room temperature for three months [Fig. 2(b)], suggesting that the structure was stable in application conditions. Meanwhile, the complex elements of Eu, B, C, and H can be caught by the EDS. The results indicated that the Eu-MOF had been prepared successfully.

To investigate the effect of the concentration of reactants, we reduced the content of $EuCl_3$ and BBDC with a certain solvent. The above structure was obtained, when $EuCl_3 \cdot 6H_2O$ (0.015 mM) and BBDC (0.015 mM) were selected. The optimized solution was prepared by dispersing the 2-mg Eu-MOF into 1-mL deionized water. A certain amount of GA was dissolved in anhydrous ethanol to obtain analysis solutions with a concentration of 1 nM–20 nM. The Eu-MOF solution of 1 mL was mixed with the GA solution. After diluted with water and mixed thoroughly, the system was transferred to a quartz cuvette for detection under a xenon lamp at room temperature. The concentration-dependent FL sensing investigation was accomplished by adding the mixture to the suspension of the Eu-MOF and GA with a final volume of 2 mL. The FL spectra with excitation at 270 nm were recorded in the range of 410 nm–800 nm by the slit widths of 5 nm. Each sample was measured at least three times, and the average value was obtained before conducting the following sample to ensure the reliability of the experimental results. Herein, we optimized experimental factors and successfully synthesized the Eu-MOF hollow spheres with Eu^{3+} as the metal node and BBDC as the ligand.

3. Results and discussion

3.1 Study on the optical performance of Eu-MOF

The photoluminescence emission spectra of the sensor were recorded and agreed well with the reported characteristic patterns of the Eu-MOF using Eu^{3+} as the metal node and BBCD as the ligand [23]. Upon the addition of GA, there was FL enhancement at 434 nm, and the emissions at 605 nm and 695 nm became weaker, corresponding to the emissions from BBDC and Eu^{3+}, respectively [Fig. 3(a)]. When the GA concentration increased, the distinct ratio metric signal change could be observed. To further validate the sensor response to GA, the selectivity of the Eu-MOF in chemical systems with the presence of various interferents was investigated. The recorded data illustrated that no significant FL signal changes of the sensor in the presence of common amino acid and metal ions from sweat were observed except GA (Fig. S1). The result showed that the sensor was highly selective to response GA, and the selectivity was attributed to the boric moiety, which is a typical functional group used to recognize the α-hydroxycarboxylic structure in GA [24]. Meanwhile, the FL intensity of the sensor reached the maximum within 7 min, presenting the satisfactory and stable response to GA during the period of the reaction kinetic test [Fig. 3(b)]. Subsequently, the quantity of hydrogen (pH) effect on the FL response of Eu-MOF in the presence and absence of GA was investigated. As shown in Fig. 3(c), the FL efficiency of the sensor achieves the maximum at pH = 7, and then declines with the increase in the values of pH in the presence of GA, because GA is a kind of acid whose oxidation reaction involves the participation of protons [25–27]. Subsequently, the effect of pH on the sensor was explored in the range of 5–8 [Fig. S2(b)]. The data showed the optimal pH was 7.4, suggesting that the Eu-MOF can detect GA in the biological environment.

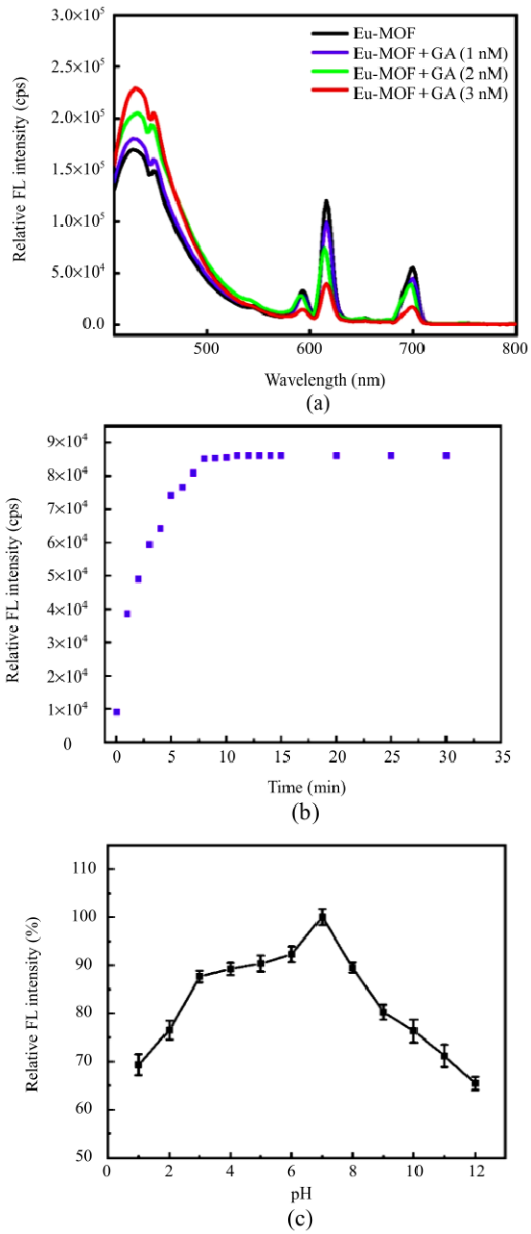

Fig. 3 Optical performance of Eu-MOF: (a) FL spectra of Eu-MOF in the absence and presence of GA, (b) kinetic curve of Eu-MOF detecting GA, and (c) FL intensity of the sensor corresponding to different pH buffer solutions of the sensor.

3.2 Optimization of the parameters

The FL signals of the sensor for GA at different excitation wavelengths were tested by orthogonal experiments, and the optimal parameter of 270 nm was selected. As shown in Fig. 4(a), with the antenna effect procedure, BBDC, as the ligand absorbs photons and produces its triplet state with the help of the intersystem crossing procedure. And then, the Eu^{3+} (D_0) was triggered to conduct energy transition (ET) among gaps accompanying FL emissions. Echoing this, the sensor of the boric-acid-functional Eu-MOF exhibited the significant linearity in the concentration range of 1 nM–2 nM GA with the detection limit of the increase of 0.34 nM ($3\sigma/S$). It was reported that human sweat contains GA, whose concentration is more than 1 μM [28–31]. Compared with the detection limit of Eu-MOF for GA (0.34 nM), we believe that the strategy could be used in visualizing LFPs.

3.3 Applications

At first, the performance of the MOF in applications was validated with imprinted fingerprints in this study. The volunteers were required to ingest equal amounts of pu-erh tea at a fixed location throughout the sample collection period of 3 months to obtain the fingerprint samples containing GA. It has been reported in the literature that the amount of GA in pu-erh tea is significantly increased due to the de-esterification of the 3-galloyl-substituted catechins by either native esterase or oxidative degradation during fermentation [32–34]. According to the structure of the skin, the sweat pores secreting fluids are distributed on the friction ridges of the fingerprints, but not at the furrow. Therefore, sweat LFPs were revealed with the high contrast by the sensor signal in the response to GA, which can only be captured in the friction ridges. Remarkably, by virtue of its appropriate energy levels, the MOF exhibited excellent photo-modulated FL switch properties and “turn-on” sensitization LFPs with high contrast between friction ridges and furrows. This paved the way toward an effective strategy for constructing a multifunctional Ln-MOF used as sensors for developing fingerprints.

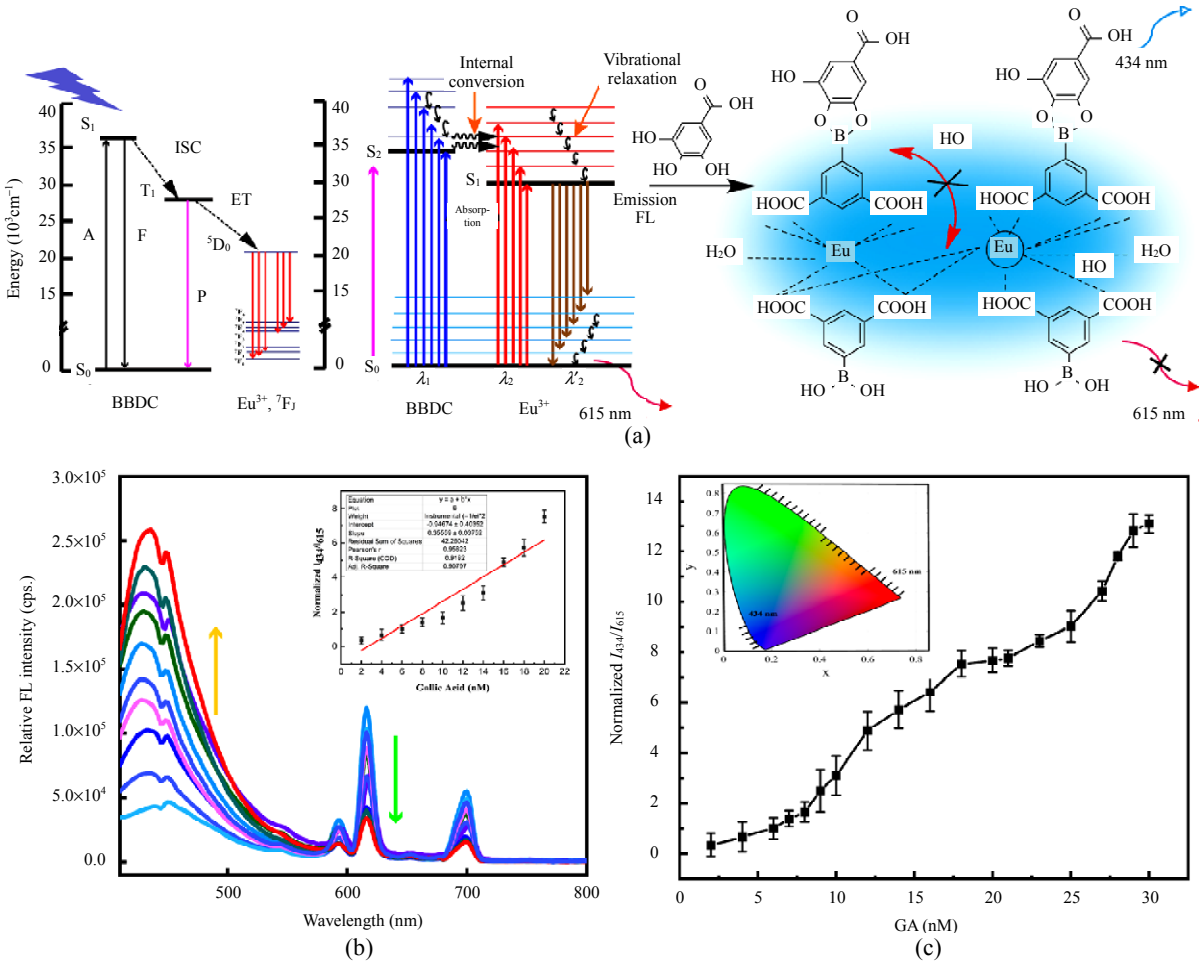

Fig. 4 Fluorescence spectra of Eu-MOF with the stepwise addition of GA under the single excitation at 270 nm: (a) schematic illustration of the absorption, migration, and emission from Eu-MOF with the antenna effect procedure (ISC for intersystem crossing; S for singlet; T for triplet; A for absorption; F for FL; P for phosphorescence; D and F for the symbols of energy levels); (b) the FL profiles of the Eu-MOF detecting different concentrations of GA (from 2 nM to 20 nM), and the linear relationship of I_{434nm}/I_{615nm} and the GA concentration: there is a good linear relationship in the range of 2 nM to 20 nM. The calibration curve is $y=-0.946\,74+4513.3x$ (R^2=0.918 2) with the low detection limit of 0.34 nM based on $3\sigma/S$; (c) chromaticity diagram (CIE): the chromaticity coordinates of Eu-MOF with the addition of GA at different concentrations and the plot of the intensity ratio of I_{434}/I_{615} vs. the GA concentration. The Eu-MOF and GA were mixed thoroughly by a vortex shaker for 1 min before imaging. Scale bar = 10 μm. The values are the mean ± S for $n=3$, where S is the standard deviation.

To further investigate the reproducibility of the sensor detecting GA in the LFP samples, 1 200 samples were collected from 12 volunteers. The volunteer's hands were not treated with any additional treatment before imprinting, keeping the normal oil-sweat mixture. Three fingerprints of the index/middle/ring finger were printed on the designated area of the porous surface with six times in succession for 45 seconds. The obtained samples were placed in the lab at room temperature, and the Eu-MOF solution was sprayed evenly by the self-made atomizing device at a distance of 20 cm. Compared with the control group without drinking tea, the impressed samples from the experimental group showed better results in the developing process. The relevant results are integrated into Fig. 5.

Based on the pre-experiment, the stability of the sensor was explored in the application for visualizing fingerprints. The samples were collected by the standard process and stored under ambient conditions for three months. The time-varying images were captured by confocal FL microscopy and quantized by the software. As shown in

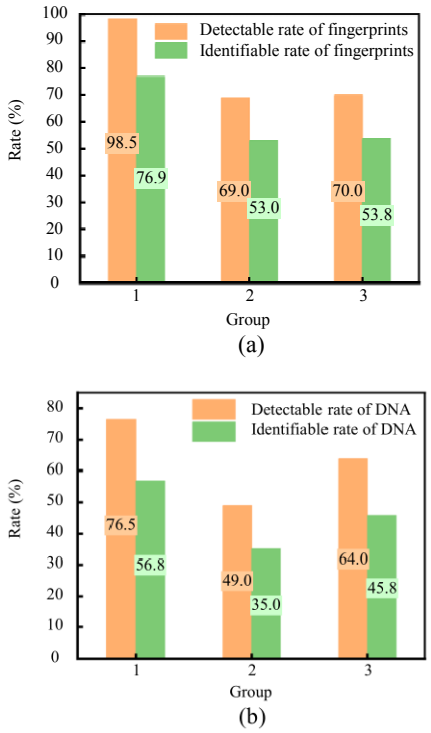

Fig. 5 Histogram of the results: yellow and green sectors are corresponding to the detectable rate (detectable samples/total samples) and identifiable rate (identifiable samples/total samples), respectively. The samples that showed ridge patterns were named by detectable samples, and the samples called identifiable samples were enough for individualization. Group 1 is the results of the experimental group, Group 2 is the results of the control group, and Group 3 shows the ratios of the identifiable samples of the above two groups samples to the total detectable samples: (a) fingerprints and (b) deoxyribonucleic acid (DNA).

Fig. 6(a), no significant changes in the brightness from fingerprints are observed by the naked eyes, and the quantitative data show that the intensity of materials is relatively steady without sharp FL decay after three months. Moreover, three levels of detailed information on the ridge pattern were also clearly distinguished, providing reliable evidence for individualization. It should be explained that in order to enhance the contrast for easy observation, in practice we tend to observe through the filter (525 nm) in the police portable laser system, and thus the fingerprint images given in the article are presented as yellow-green light. From Fig. 7, the images are magnified to capture the details of the fingerprint. The FL pixel profiles of LFPs on the porous object show obvious contrast between friction ridges and furrows, enabling the fingerprint to be clearly distinguished [Figs. 6(b) and 7(d)]. The yellow line in Fig. 7(d) clearly depicts the contrast of the FL signal between the furrow and the friction ridge, exhibiting that microscopic fingerprint ridge details (Levels 2 and 3) are also extracted in the high resolution images. Unlike the reported LFPs imaging through the interaction with proteins or lipids in sweat, the LFPs through the chemically stable GA were easier to retain for a long time, which was conducive to the subsequent biological information analysis. It should be added that the Level 2 details, also known as the minutiae, are the endpoints of each friction ridge and the combination with the adjacent lines or bars, named as the beginning, ending, bifurcation, connecting, hook, enclosure, bridge, line, and dot. The friction ridge is the outer epidermal protrusion of the palmar surface of the hand or foot. The furrow is a concave subdivision between the raised friction ridges. The sweat pores are located on the friction ridge as well as the above ridge pattern, which is revealed in this article.

The results showed that LFPs were revealed by the boric-acid-fabricated Eu-MOF sensor. Referring to the unified forensic science workflow, we extracted the DNA of the above samples in the standard extraction process. The obtained short tandem repeats (STR) profiles were identified by professional examiners as matched, suggesting that the DNA detection would not be affected obviously after the visualization operation of the sensor [Fig. 6(c)]. The result verified the application potential of the visualization strategy in the forensic science.

Based on the above, the boric-acid-fabricated Eu-MOF sensor showed the good stability in the progress, which made it successfully applied for visualizing the LFP by the selectivity to GA. Notably, we investigated the impact of the revealed method on subsequent DNA detection. The DNA from the above 1200 samples was collected by the

direct clipping method. The data results are presented in the form of Fig. 5(b). Corresponding DNA control samples from the same source were obtained by wiping the upper chamber of the volunteer's mouth back and forth with a cotton swab for five times. To accord with the practical techniques in the forensic science, 16 characteristic genetic motifs were examined in this paper. One of the STR profiles was presented to illustrate the matched results in Fig. 6(c).

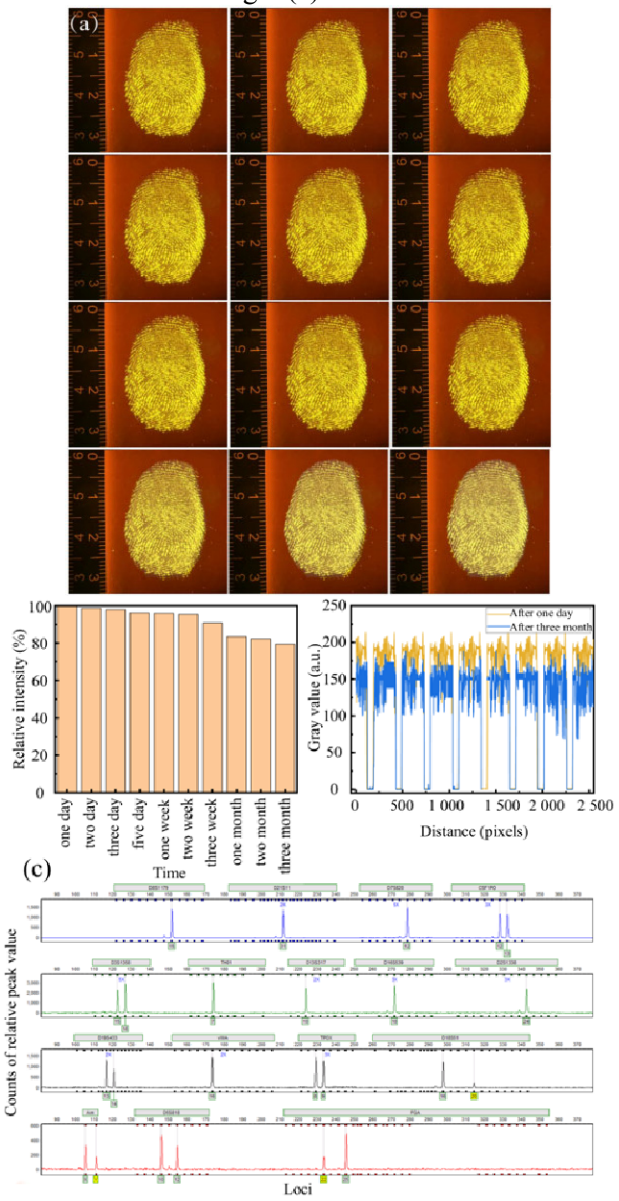

Fig. 6 Fingerprint photographs and the pixel profile: (a) time-dependent fingerprints, (b) fluorography quantified by pixel values with different aging time from one day to three months, and (c) DNA detection results after the visualization progress.

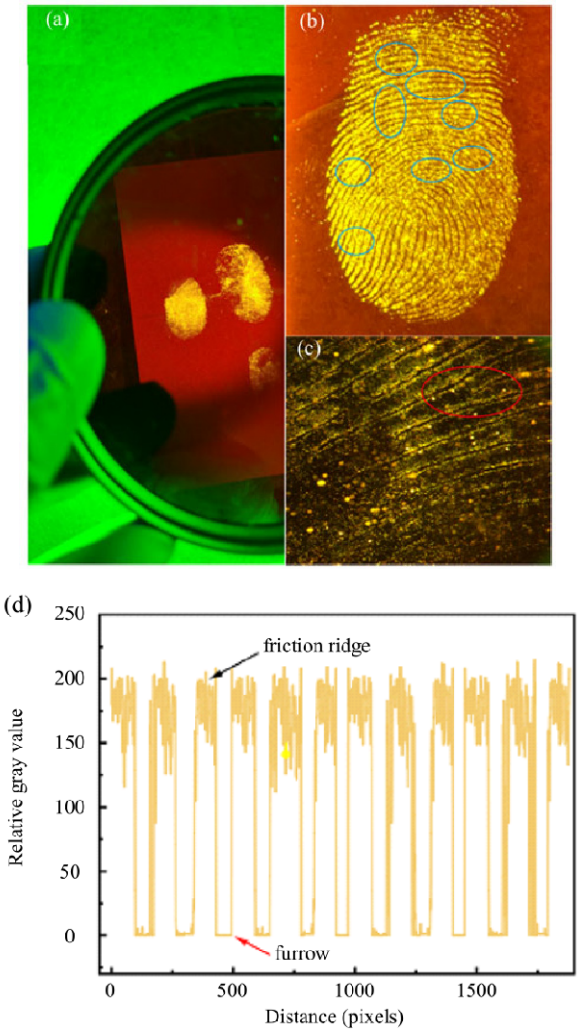

Fig. 7 Details of the fingerprint: (a) schematic diagram, (b) and (c) two-photon microscopy (TPM) images of fingerprints, and (d) pixel profile of the corresponding selected area in the developed fingerprints.

Given the complexity of the case scene, we simulated the pseudo-operational trial to evaluate such process on more operationally representative materials. The notebook covers, kraft envelopes, and printing papers in daily life from the volunteer were collected as the practical samples. The obtained fingerprint images and the DNA extraction results from the corresponding locations were selected to show in Figs. 8(a)–8(d). As shown in Figs. 8(a)–8(c), only part of the ridge patterns in fingerprints and six loci in the DNA profiles are presented, indicating not enough to realize individualization. Although the results were undesirable, the above data

demonstrated that the sensor could be regarded as the suitable and competitive sensor for revealing LFPs on porous objects by the photoluminescence strategy.

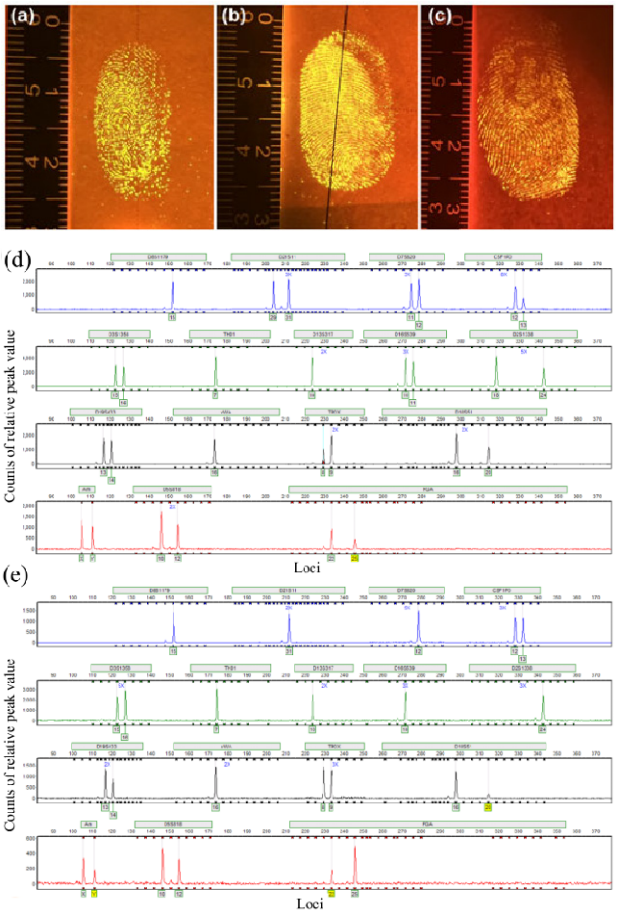

Fig. 8 Visualizing results in test objects: (a) printing paper, (b) notebook cover, (c) kraft paper envelopes, (d) DNA profile of the selected volunteers, and (e) DNA detection results after the visualization operation.

4. Conclusions

In this work, the boric-acid-functional Eu-MOF was successfully fabricated for detecting GA sensitively to visualize the LFPs. Under optimized conditions, the proposed sensor exhibited the significant ratiometric fluorescent signal with the addition of GA, showing the desirable linearity with a low detection limit of 0.34 nM. Relying on the good performance of the sensor, the developed fingerprints exhibited the high contrast and superior stability without background interference. Of particular importance was that we conducted the pseudo-operational trial to prove that the method had less impact on the subsequent DNA detection. In summary, the potential of the sensor to reveal biological information and morphological patterns from LFPs was foreseen, providing the application prospect of the sensor in the field of forensic science.

Supplementary materials

S.1 Materials and instruments

The BBDC was provided by Shanghai Macklin Biochemical Co. Ltd., China. GA; europium chloride hexahydrate ($EuCl_3 \cdot 6H_2O$, AR); DMF, AR; anhydrous ethanol (99.5% pure, with molecular sieve, water $\leq$ 50 ppm) were obtained by Sigma-Aldrich Co. Ltd., China. Other reagents were supplied by CAS Mart, China. The ultrapure water was prepared through a milli-*Q* integral water purification system (Edinburgh Instruments, UK). The Identifiler^{TM} plus amplification kit was used in this process (Thermo, USA, including 15 autosomal loci and one sex locus). And the others adopted in this work included: the Qubit® dsDNA HS assay DNA quantification kit (Invitrogen, USA), internal standard LIZ500 (Thermo, USA), deionized formamide (Thermo, USA), and standard reference ladder (Thermo, USA). All chemical reagents and solvents were used without further purification, unless otherwise mentioned.

The photoluminescence spectrometer (Edinburgh FLS1000, UK) was used to record the FL spectra of the Eu-MOF. The ultraviolet-visible spectrum (UV) absorption spectra of Eu-MOFs were recorded on a UV-visible spectrophotometer (Thermo Scientific Biomate 3S, USA). The zeta potential and particle size were measured by Zetasizer Nano ZS90 (Malvern, UK). The powder X-ray diffraction (PXRD) was achieved by Thermo Escalab 250XI, USA; X-ray photoelectron spectroscopy (XPS) Tescan Mira LMS, Czech Republic); vibrating sample magnetometer VSM

LakeShore7404, USA. The morphology, elemental distribution map, and EDS of the products were observed by the scanning electron microscopy (SEM, Thermo Scientific FEI Talos F200X G2, Czech Republic) and transmission electron microscope (JEM-2100F, Japan). X-ray powder diffraction (XRD) patterns of the samples were achieved on a Bruker D8 advanced X-ray diffractometer ($Cu_{k\alpha}$ radiation and $\lambda = 1.541\ 8$ Å), using a generator with a voltage of 40 kV and a current of 40 mA. All FL photographs were taken with the Canon EOS600D digital camera under Tech-Long multi-band forensic laser systems (a portable laser) at 525 nm. Besides, the LSM 880 NLO two-photon laser scanning confocal microscope (Zeiss, Germany), micro biological evidence DNA extraction and purification system (Changchun Bokun Biotechnology Co. Ltd., China), Proflex™ PCR amplification instrument (Thermo, USA), ABI 3500XL (Applied Biosystems, USA), GA118-24B genetic analyzer, and Gene Marker® DNA result analysis software (Soft Genetics, USA) were also used in this work.

S.2 Optical properties and optimization

The emission monitoring at 434 nm for the selectivity of the Eu-BBDC@MOF sensor is shown in Fig. S1. And leucine, alanine, glycine, valine, serine, phenylalanine, histidine, tyrosine, isoleucine, and tryptophan are the common amino acid in the human sweat; proline, wax ester, creatinine, choline, lactic acid, urea, and uric acid are the organic substances in the sweat; Na^+, Cl^-, S^{2-}, K^+, Ca^{2+}, and PO_4^{3-} are the most abundant metal ions in the human sweat.

The effect of pH on the Eu-MOF sensor performance is shown in Fig. S2. And the optical performance of the sensor is shown in Fig. S3.

The quantum yield (QY) measurement of Eu-BBDC@MOF in the aqueous solution was calculated according to the slope method, as shown in Fig. S4, where the quinine sulfate in 0.1 M H_2SO_4 (QY = 2.93%) was employed as the standard. The equation $\varphi_x = \varphi_{st}(K_x/K_{st})(\eta_x/\eta_{st})^2$ was used to calculate the QY, where φ is the QY, K is the slope, and η is the refractive index; the subscript "st" refers to the standards (quinine sulphate) and "x" refers to the unknown samples. For these aqueous solutions, $\eta_x/\eta_{st} = 1$.

In Fig. S5, I_{434} and I_{615} mean the emission intensity values at 434 nm and 615 nm, respectively. It is observed from Fig. S5 that Eu-MOF exhibited ideal reproducibility. And the relative standard deviation (RSD) is inserted in the figure.

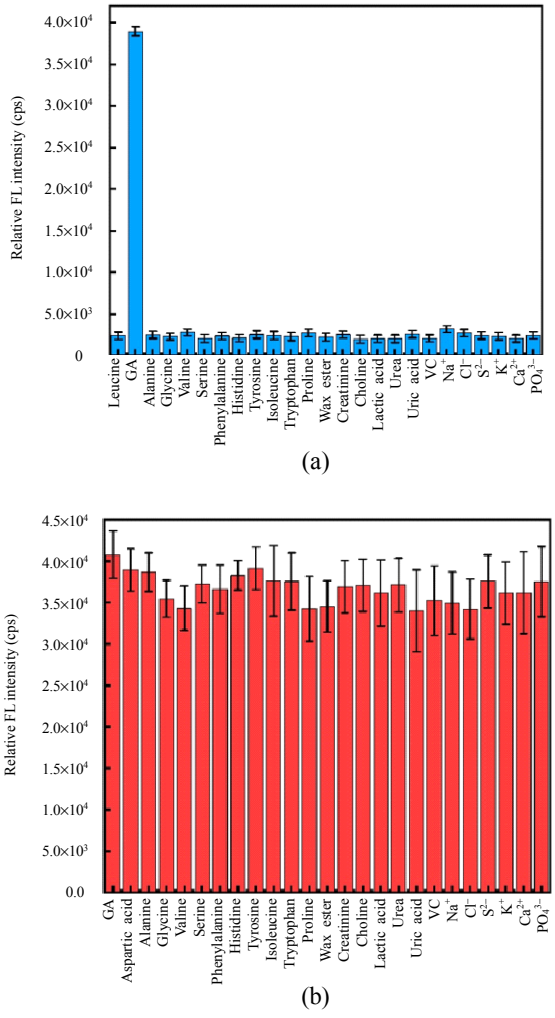

Fig. S1 Emission monitoring at 434 nm for the selectivity of the Eu-BBDC@MOF sensor: (a) emission spectra upon various interferents with only Eu-BBDC@MOF sensor added and (b) reaction system of Eu-BBDC@MOF sensor mixed GA.

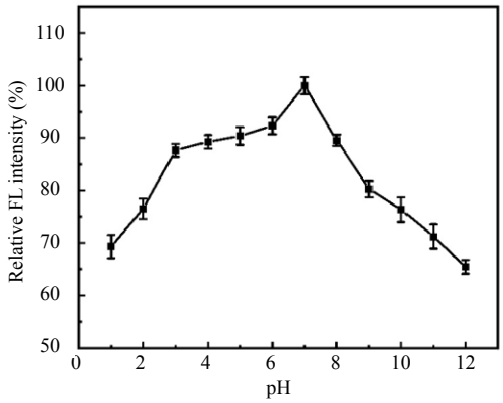

Fig. S2 Effect of pH on the Eu-MOF sensor performance. Error bars represent the standard deviations detected for three parallel experiments.

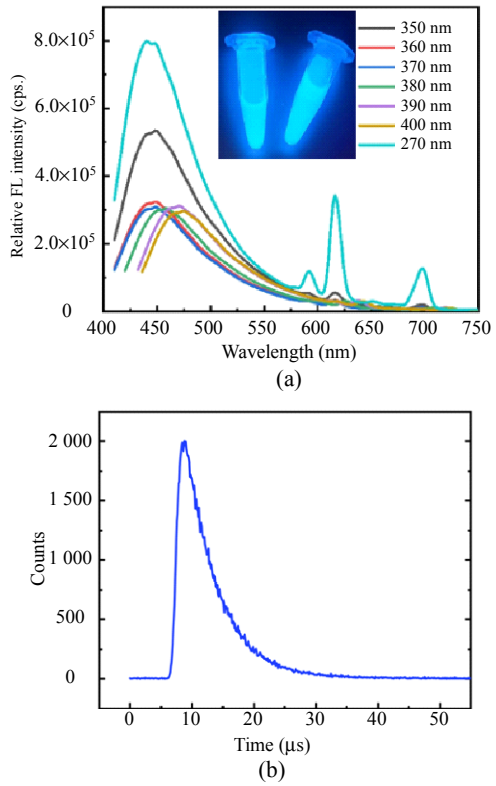

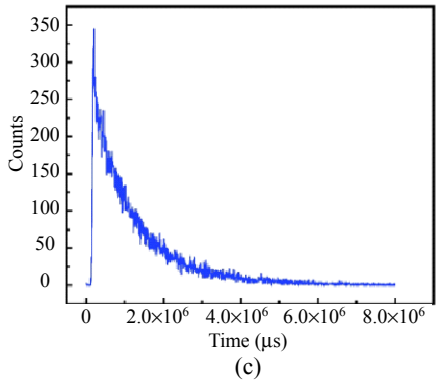

Fig. S3 Optical performance of the sensor: (a) emission spectra of the reaction system under the different excitation wavelengths; (b) and (c) the decay lifetime curves.

Quantum yield results
for "Multi Scans (QY)"

Scatter range: 270.00 to 300.00 nm
Emission range: 320.00 to 700.00 nm

QY = 2.93%

Fig. S4 QY results.

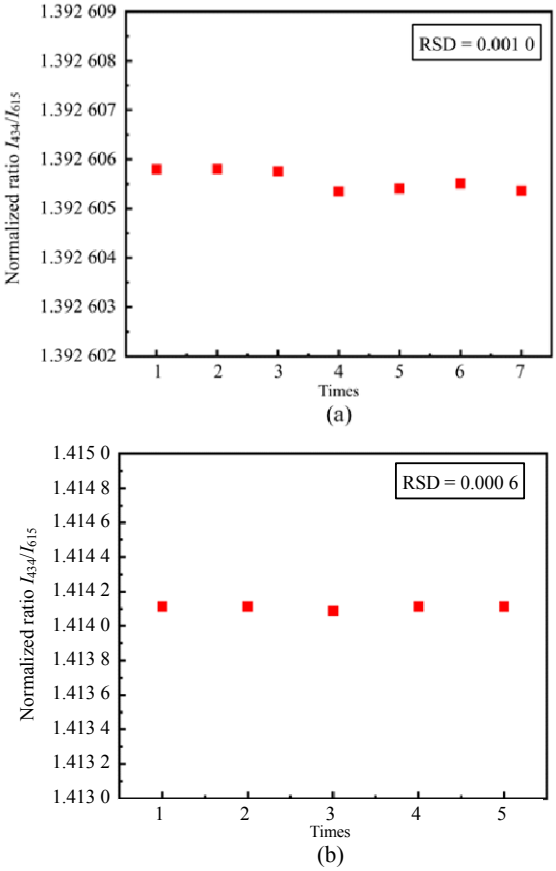

Fig. S5 Repeatability testing: normalized intensity of the FL signal: (a) the scatter plot of seven times of repetitive measurement with the same Eu-MOF responding to 200 nM of GA and (b) the scatter plot of the same concentration of GA with five independent times.

S.3 Cell culture

The Rattus norvegicus, the rat cell line (H9C2 myoblasts, which is a cell model used as an alternative for cardiomyocytes), were grown in the Dulbecco's modified eagle medium (DMEM) with 1% 100 U·mL^{-1} antibiotics penicillin/streptomycin and 10% fetal bovine serum (FBS) at 37 ℃ under a humidified atmosphere containing 5% CO_2.

S.4 3-(4,5)-dimethylthiahiazo(-z-y1)-3,5-di-phenytetrazoliumromide (MTT) assay

To demonstrate the safety of the Eu-MOF, the cytotoxicity of the Eu-MOF was tested in H9C2 cells using a standard MTT assay. The IC_{50} value is shown in Fig. S6.

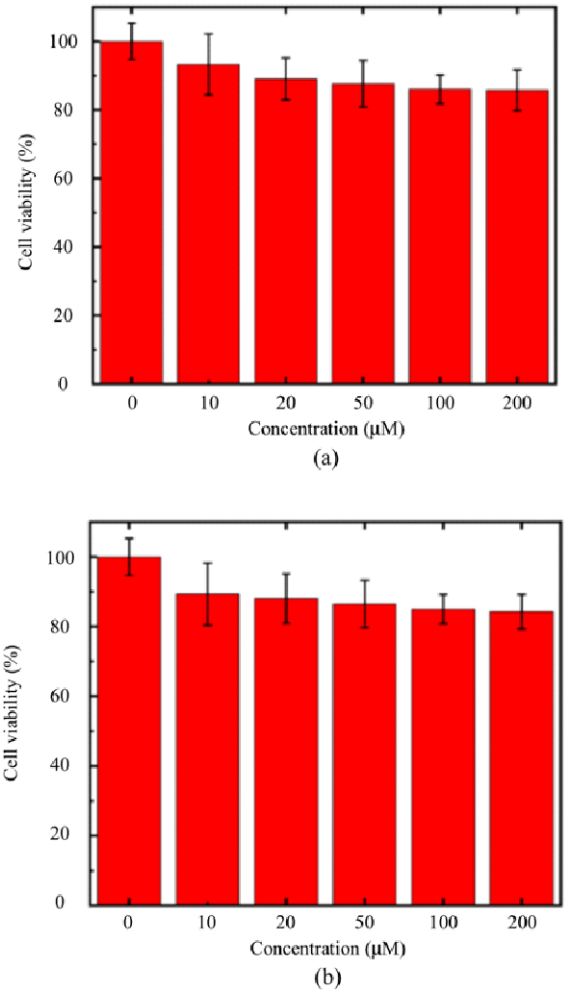

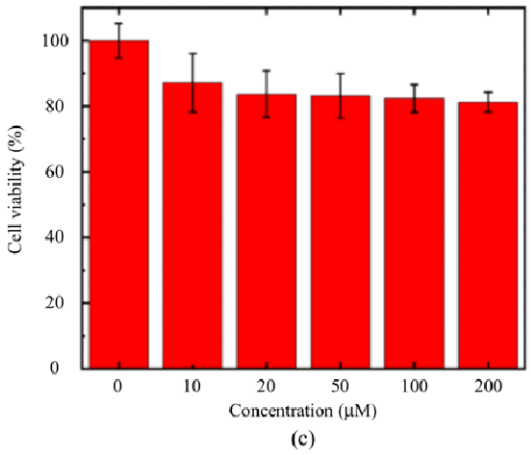

Fig. S6 Result of cytotoxicity assay for different incubation time for the sensor and cells, respectively (H9C2 myoblasts with low proliferative capacity were selected as a cell model in this work): (a) 24 h, (b) 48 h, and (c) 72 h.

The IC_{50} value was calculated according to the method of Huber and Koella [35]. In Fig. S6, it is displayed that the value of IC_{50} is calculated as 236.7 μg·mL^{-1} for the Eu-MOF, which indicates the good biocompatibility for fingerprints imaging.

Acknowledgment

The authors would like to thank the sample volunteers for their constant support, the editorial office, and anonymous reviewers whose helpful comments improved the quality of this paper.

The work was supported by the People's Public Security University of China Double Class Innovative Research Special Project on Criminal Science and Technology (Grant No. 2023SYL06).

Declarations

Ethics Approval and Consent to Participate The experimental processes were supervised by People's Public Security University of China, China. And all the volunteers have signed the informed consent before data collection. All approaches performed in the study involving data collection and storage were followed according to the standard operation process of the Fingerprint Imag e Capture Technical Specifications (GA/T 625-2010, China).

Conflict of Interest The authors declare that they have no competing interests.

References

[1] B. T. Ulery, R. A. Hicklin, G. I. Kiebuzinski, M. A. Roberts, and J. Buscaglia, "Understanding the sufficiency of information for latent fingerprint value determinations," *Forensic Science International*, 2013, 230(1–3): 99–106.

[2] A. de Ronde, B. Kokshoorn, C. J. de Poot, and M. de Puit, "The evaluation of fingermarks given activity level propositions," *Forensic Science International*, 2019, 302: 109904.

[3] K. J. Sheridan, E. Saltupyte, R. Palmer, and M. D. Gallidabino, "A study on contactless airborne transfer of textile fibres between different garments in small compact semi-enclosed spaces," *Forensic Science International*, 2020, 315: 110432.

[4] S. Bennett, C. P. Roux, and J. Robertson, "The significance of fibre transfer and persistence – a case study," *Australian Journal of Forensic Sciences*, 2010, 42(3): 221–228.

[5] R. Palmer, K. Sheridan, J. Puckett, N. Richardson, and W. Lo, "An investigation into secondary transfer – the transfer of textile fibres to seats," *Forensic Science International*, 2017, 278: 334–337.

[6] M. Calderón-Santiago, F. Priego-Capote, B. Jurado-Gámez, and M. D. Luque de Castro, "Optimization study for metabolomics analysis of human sweat by liquid chromatography-tandem mass spectrometry in high resolution mode," *Journal of Chromatography A*, 2014, 1333: 70–78.

[7] J. Iglesias, I. Medina, M. Pazos. R. Watson, V. R. Preedy, and S. Zibadi, "*Polyphenols in Human Health and Disease*," San Diego: Academic Press, 2014: 323–338.

[8] T. D. James, K. R. A. S. Sandanayake, and S. Shinkai, "Saccharide sensing with molecular receptors based on boronic acid," *Angewandte Chemie International Edition in English*, 1996, 35(17): 1910–1922.

[9] S. Meng, G. Li, P. Wang, M. He, X. Sun, and Z. Li, "Rare earth-based MOFs for photo/electrocatalysis," *Materials Chemistry Frontiers*, 2023, 7(5): 806–827.

[10] L. D. Carlos, R. A. S. Ferreira, V. de Z. Bermudez, and S. J. L. Ribeiro, "Lanthanide-containing light-emitting organic-inorganic hybrids: a bet on the future," *Advanced Materials*, 2009, 21(5): 509–534.

[11] P. P. Lima, F. A. Almeida Paz, R. A. S. Ferreira, V. de Zea Bermudez, and L. D. Carlos, "Ligand-assisted rational design and supramolecular tectonics toward highly luminescent Eu^{3+}-containing organic-inorganic hybrids," *Chemistry of Materials*, 2009, 21(21): 5099–5111.

[12] A. A. Ansari, J. P. Labis, and A. Khan, "Facile synthesized NaGdF4:Yb,Er peanut - shaped, highly biocompatible, colloidal upconversion nanospheres," *Luminescence*, 2022, 37(7): 1048–1056.

[13] D. Yang, J. Xu, G. Yang, Y. Zhou, H. Ji, H. Bi, *et al.*, "Metal-organic frameworks join hands to create an anti-cancer nanoplatform based on 808 nm light driving up-conversion nanoparticles," *Chemical Engineering Journal*, 2018, 344: 363–374.

[14] L. Zhao, X. Song, X. Ren, H. Wang, D. Fan, D. Wu, *et al.*, "Ultrasensitive near-infrared electrochemiluminescence biosensor derived from Eu-MOF with antenna effect and high efficiency catalysis of specific CoS_2 hollow triple shelled nanoboxes for procalcitonin," *Biosensors and Bioelectronics*, 2021, 191: 113409.

[15] L. Song, J. Xiao, R. Cui, X. Wang, F. Tian, and Z. Liu, "Eu^{3+} doped bismuth metal-organic frameworks with ultrahigh fluorescence quantum yield and act as ratiometric turn-on sensor for histidine detection," *Sensors and Actuators B: Chemical*, 2021, 336: 129753.

[16] J. Wu, Y. Li, B. Song, C. Zhang, Q. Wang, X. Gao, *et al.*, "Microstructured optical fiber based on surface plasmon resonance for dual-optofluidic-channel sensing," *Plasmonics*, 2022, 17(5): 1965–1971.

[17] S. Ben Zakour and H. Taleb, "Shift endpoint trace selection algorithm and wavelet analysis to detect the endpoint using optical emission spectroscopy," *Photonic Sensors*, 2016, 6: 158–168.

[18] L. Pei, W. Zhang, S. Yang, K. Chen, X. Zhu, Y. Zhao, *et al.*, "Nitrogen and sulfur Co-doped carbon dots as a turn-off fluorescence probe for the detection of cerium and iron," *Journal of Fluorescence*, 2023, 33(3): 1147–1156.

[19] X. Qiao, Y. Han, D. Tian, Z. Yang, J. Li, and S. Zhao, "MOF matrix doped with rare earth ions to realize ratiometric fluorescent sensing of 2,4,6-trinitrophenol: synthesis, characterization and performance," *Sensors and Actuators B: Chemical*, 2019, 286: 1–8.

[20] X. Jiang, H. Jin, Y. Sun, Z. Sun, and R. Gui, "Assembly of black phosphorus quantum dots-doped MOF and silver nanoclusters as a versatile enzyme-catalyzed biosensor for solution, flexible substrate and latent fingerprint visual detection of baicalin," *Biosensors and Bioelectronics*, 2020, 152: 112012.

[21] L. Sun, Y. Zhang, X. S. Lv, and H. D. Li, "A luminescent Eu-based MOFs material for the sensitive detection of nitro explosives and development of fingerprint," *Inorganic Chemistry Communications*, 2023, 156: 111267.

[22] Z. Sun, Y. Li, Y. Ma, and L. Li, "Dual-functional recyclable luminescent sensors based on 2D lanthanide-based metal-organic frameworks for highly sensitive detection of Fe^{3+} and 2,4-dinitrophenol," *Dyes and Pigments*, 2017, 146: 263–271.

[23] Y. Cui, F. Chen, and X. B. Yin, "A ratiometric fluorescence platform based on boric-acid-functional Eu-MOF for sensitive detection of H_2O_2 and glucose," *Biosensors and Bioelectronics*, 2019, 135: 208–215.

[24] L. R. Fitzpatrick and T. Woldemariam, "*Comprehensive Medicinal Chemistry III*," Berlin: Elsevier, 2017: 495–510.

[25] J. Li, Y. Yang, Y. Li, P. Zhao, J. Fei, and Y. Xie, "Detection of gallic acid in food using an ultra-sensitive electrochemical sensor based on glass carbon electrode modified by bimetal doped carbon nanopolyhedras," *Food Chemistry*, 2023, 429: 136900.

[26] M. Badea, F. di Modugno, L. Floroian, D. M. Tit, P. Restani, S. Bungau, *et al.*, "Electrochemical strategies for gallic acid detection: potential for application in clinical, food or environmental analyses," *Science of the Total Environment*, 2019, 672: 129–140.

[27] A. Terbouche, S. Boulahia, S. Mecerli, C. Ait-Ramdane-Terbouche, H. Belkhalfa, D. Guerniche, *et al.*, "A novel hybrid carbon materials-modified electrochemical sensor used for detection of gallic acid," *Measurement*, 2022, 187: 110369.

[28] G. Bart, D. Fischer, A. Samoylenko, A. Zhyvolozhnyi, P. Stehantsev, I. Miinalainen, *et al.*, "Characterization of nucleic acids from extracellular vesicle-enriched human sweat," *BMC Genomics*, 2021, 22(1): 425.

[29] N. Kahkeshani, F. Farzaei, M. Fotouhi, S. S. Alavi, R. Bahramsoltani, R. Naseri, *et al.*, "Pharmacological effects of gallic acid in health and diseases: a mechanistic review," *Iranian Journal of Basic Medical Sciences*, 2019, 22(3): 225–237.

[30] A. Serag, Z. Shakkour, A. M. Halboup, F. Kobeissy, and M. A. Farag, "Sweat metabolome and proteome: recent trends in analytical advances and potential biological functions," *Journal of Proteomics*, 2021, 246: 104310.

[31] S. J. Montain, S. N. Cheuvront, and H. C. Lukaski, "Sweat mineral-element responses during 7 h of exercise-heat stress," *International Journal of Sport Nutrition and Exercise Metabolism*, 2007, 17(6): 574–582.

[32] B. Caballero, P. M. Finglas, and F. Toldrá, "*Encyclopedia of Food and Health*," Salt Lake City: Academic Press, 2016: 268–272.

[33] F. Liu, Y. Wang, H. Corke, and H. Zhu, "Dynamic changes in flavonoids content during congou black tea processing," *LWT*, 2022, 170: 114073.

[34] A. Shevchuk, R. Megías-Pérez, Y. Zemedie, and N. Kuhnert, "Evaluation of carbohydrates and quality parameters in six types of commercial teas by targeted statistical analysis," *Food Research International*, 2020, 133: 109122.

[35] W. Huber and J. C. Koella, "A comparison of three methods of estimating EC_{50} in studies of drug resistance of malaria parasites," *Acta Tropica*, 1993, 55: 257–261.